Articles in PresS. J Neurophysiol (August 18, 2010). doi:10.1152/jn.00076.2010

NEURAL SUBSTRATE OF AN INCREASE IN SENSORY SAMPLING TRIGGERED BY A MOTOR COMMAND IN A GYMNOTID FISH.

Virginia Comas and Michel Borde

Laboratorio de Neurofisiología Celular y Sináptica

Dpto. de Fisiología, Facultad de Medicina.

Universidad de la República.

Gral. Flores 2125.

11800 Montevideo, URUGUAY.

Running head: **Increased sensory acquisition during escape.**

Corresponding author: Michel Borde, Dpto. de Fisiología, Facultad de Medicina. Gral. FLORES 2125, CP 11800, Montevideo, URUGUAY. Phone: 598-2-924 3414 ext. 3343. Fax: 598-2-924 8732. E-Mail: mborde@fmed.edu.uy

ABSTRACT

Despite recent advances that have elucidated the effects of collateral of motor commands on sensory processing structures, the neural mechanisms underlying the modulation of active sensory systems by internal motor-derived signals remains poorly understood. This paper deals with the neural basis of the modulation of the motor component of an active sensory system triggered by a central motor command in a gymnotid fish. In *Gymnotus omarorum*, activation of Mauthner cells, a pair of reticulospinal neurons responsible for the initiation of escape responses in most teleosts, evokes an abrupt and prolonged increase in the rate of the electric organ discharge (EOD), the output signal of the electrogenic component of the active electrosensory system. We show here that prepacemaker neural structures (PPs) that control the discharge of the command nucleus for EODs, are key elements of this modulation. Retrograde labeling combined with injections of glutamate at structures that contain labeled neurons showed that PPs are composed of a bilateral group of dispersed brainstem neurons that extend from the diencephalon to the caudal medulla. Blockade of discrete PPs regions during the Mauthner cell-initiated electrosensory modulation indicate that the long duration of this modulation relied on activation of diencephalic PPs whereas its peak amplitude depended on the recruitment of medullary PPs. Temporal correlation of motor and sensory consequences of Mauthner cell activation suggests that the Mauthner cell-initiated enhancement of electrosensory sampling is involved in the selection of escape trajectory.

INTRODUCTION

Since the pioneering work of Sperry (1950) and von Holst and Mittelstaedt (1950), the idea of a modulation of sensory processing exerted by internal collaterals of motor signals has been commonly accepted. This kind of internal signals, known as corollary discharges (CD) or efference copies, has been widely implicated in the cancellation of self-generated sensory feedback during movement and other behaviors (McCloskey 1981). For example, in weakly electric mormyrid fishes, many mechanisms by which the motor command cancels the sensory feedback in hindbrain circuits have been elucidated (Bell 1989; Sawtell et al. 2005). The situation in the natural world, however, may require more complex interactions than simple cancellation (Crapse and Sommer 2008; Nelson and MacIver 2006; Poulet and Hedwig 2006; Sommer and Wurtz 2008). Indeed, motor commands may require increases or other modulations in active sensing as described for example in bats (Wilson and Moss 2004) and rats (Grant et al. 2009). These modulations could also be mediated by internal collaterals of motor commands, but these mechanisms have not been as widely investigated.

The modulation of the electrogenic component of the active electrosensory neural system triggered by a motor command described in *Gymnotus omarorum*, a pulse type gymnotiform fish (Falconi et al. 1995, 1997; Morales et al. 1993), emerged as a useful vertebrate model to analyze such high-level motor-sensory interactions. As in most weakly electric fish, the active electrosensory system in *Gymnotus omarorum* includes an electrogenic component, responsible for the emission of electric organ discharges (EODs), and an electroreceptive component devoted to the reception and processing of

sensory signals evoked by their own self-generated electric fields during each EOD (Caputi 2004; Lorenzo et al. 2001). In this species, activation of the Mauthner cells (M-cell), the command neurons for escape responses in most teleosts, triggers an abrupt and prolonged increase in EOD rate (M-AIR, an acronym for Mauthner-initiated Abrupt Increase in Rate). Although motor activity could lead to an increase in EOD rate through a feedback sensory mechanism (Lissman and Machin 1958; Barrio et al. 1991), previous work indicate a neural connection between the Mauthner system and the electrogenic component of the active electrosensory system since M-AIR still occurs under pharmacological immobilization of the fish (Curti et al. 1999, 2006; Falconi et al. 1995, 1997). Moreover, the short latency of M-cell triggered synaptic actions on pacemaker cells of the medullary pacemaker nucleus (PMn), the command nucleus for EODs (Curti et al. 2006; Falconi et al. 1997), points to a paucisynaptic neural pathway between both systems.

In most gymnotifom fish, modulations of EOD rate or waveform involve the activation of different prepacemaker structures (PPs) (Kawasaki et al. 1988; Keller et al. 1991). These structures may function as neural centers at which several processed inputs are subsequently transformed into specific modulations of the activity of the PMn (Caputi et al. 2005; Keller, et al. 1990; Lorenzo et al. 2001; Santana et al. 2001). We hypothesize that, in *Gymnotus omarorum*, PPs are also involved in the organization of the M-cell-initiated enhancement of electrosensory sampling. To test this hypothesis, PPs were first identified according to anatomical and functional criteria and effects of their specific blockade on M-AIR were assessed. Our data indicate that a set of functionally segregated PPs are key elements of this modulation and suggest

that an enhancement of electrosensory sampling triggered by M-cell activation is involved in motor sequencing during escape.

MATERIALS AND METHODS

Fifty-five juvenile specimens of *Gymnotus omarorum* nov. sp. (formerly identified as *Gymnotus carapo,* Richer-de-Forges et al. 2009) with a mean length of 16 cm (SD ± 2.8 cm) were used in this study. All experimental procedures were previously described in detail (e.g., Falconi et al. 1995); they were conducted in accord with the guidelines set forth by the Comisión Honoraria de Experimentación Animal, Universidad de la República ("Uso de animales en experimentación, docencia e investigación Universitaria", CDC Exp. 4332/99, Diario Oficial Nº 25467, Feb. 21/00).

Surgical Procedures. Fish were anaesthetized by immersion in iced water. All surgical areas and fixation points were infiltrated with Lidocaine®. During surgical procedures, the gills were perfused with aerated iced tap water. The paravertebral muscles were removed from one side of the fish at the caudal portion of the tail (at about 80% of the fish length) in order to place a bipolar stimulating electrode in contact with the vertebral column. Electrical stimuli were applied to the spinal cord using this electrode in order to determine the threshold intensity required to induce the tail flip that follows M-axon activation (see below). The dorsal surface of the brain was exposed through an opening in the skull to provide access for micropipettes used for recording and drug application at different deep brainstem structures. Following these procedures, the animals were injected with d-Tubocurarine (1-3 µg/g, i.m.) at doses that produced paralysis but did not completely eliminate the EOD. After surgical preparation and curarization, the gills were continuously perfused with aerated tap water at room temperature (20-25 ºC).

Recording and Stimulation Procedures. In most experiments the same micropipette was used for field potential recordings and drug application. Electrical recordings were obtained using micropipettes filled with NaCl (154 mM) based solutions of different compounds (see below) connected to an Axoclamp 2B amplifier (Axon Instruments, Foster City, CA, USA). A Grass Technologies (Quincy, MA, USA) P15 preamplifier was used to monitor the EOD (head to tail) with a pair of metal electrodes placed next to the fish and in contact with the supporting wet sponge, with a gain of 100x and low pass filtered (cut-off at 3 KHz). The signals were displayed on an oscilloscope and stored on magnetic tape. Data acquisition and analyses were performed using a Macintosh CI microcomputer (Apple Computers, Cupertino, CA) using specially designed software. Superscope software (GW Instruments, Somerville, MA, USA) was used to construct instantaneous frequency versus time plots.

Retrograde labeling experiments. Micropipettes were filled with a 2% solution of biocytin (Vector Laboratories, Burlingame, CA, USA) in KCl 0.5 M and were used for recording and cell marker application. Guided by the characteristic waveform of the PMn field potential (Curti et al. 2006; see Fig. 1B), biocytin was iontophoresed near pacemaker cells (PM-cells) using a PSIU6 isolation unit (Grass Technologies) delivering 500 ms pulses of 2 to 6 μA with alternate polarities at 0.5 Hz for 30-60 min. After biocytin iontophoresis, the skull was sealed with gelfoam® and dental acrylic, and the animal was allowed to survive for 2-5 days (Kawasaki et al. 1988). Animals were then deeply anaesthetized by immersion in iced water; the brains were removed and fixed overnight by immersion in paraformaldehyde (4%). Once embedded in gelatine (5% in 0.9% NaCl solution), the brains were mounted in a Vibroslicer

(Campden, Lafayette, IN, USA) and serially sliced (80 μm) at transverse or horizontal planes. Biocytin-labeled cells were visualized using the Vectastain ABC System (Vector Laboratories, Burlingame, CA, USA), based on standard procedures as described by Horikawa and Armstrong (1988). Brain sections were counterstained with Pyronin-Y Red, mounted and examined with a Nikon Optiphot microscope. Digital photographs were taken with a Kodak MDS120 camera. Labeled cells were counted by two independent observers in every case and only neurons whose somata were unequivocally labeled were included in the counts. In spite of probable minor species specific differences, nuclei and structures referred to in the description of anatomical data were defined in accord to the stereotaxic atlas of *Apteronotus*, a wave type weakly electric fish (Maler et al. 1991).

Exploration of Glu sensitivity. At brainstem locations selected according to the distribution of labeled cells, microdroplets (10-30 μm diameter measured in air) of a glutamate solution (Glu, L-glutamic acid 10 mM, dissolved in 154 mM NaCl) were applied by pressure (10-40 psi, 50-60 ms) at discrete locations, 100 μm apart, during exploratory vertical tracks using a Picospritzer II injector (General Valve Corporation, Fairfield, NJ, USA). EOD rate and waveform were monitored prior to, during and following each Glu ejection. At a given region, a series of at least 10 exploratory vertical tracks of 1500 μm were performed at two or three different distances from midline (range from 400 μm to 900 μm) and at four or five positions in the rostrocaudal axis. Although exploration of Glu sensitivity was centered in the depth range at which labeled neurons were observed, in most experiments vertical tracks also explored more superficial and ventral regions. For each vertical exploratory tract, depth series of EOD

rate modulations evoked by Glu at each ejection site were constructed. Responses were considered short latency when the first EOD interval affected by Glu ejection coincided with the interval at which ejection occurred.

Activation of Mauthner cells. M-cells axons were stimulated at the spinal cord with rectangular current pulses (0.15–0.3 mA, 0.2–0.5 ms), which were sufficient to activate both M-cell axons. This was determined by the amplitude of M-AIR (see Falconi et al. 1995) and confirmed during extracellular recordings from the left M-cell by the appearance of the characteristic sequence of electrical events produced by the activation of one or both M-cell axons (see Borde et al. 1991). In most experiments, M-cells were activated by single stimuli repeated at a low rate (every 3 min). For the experiments that were designed to study the role of medullary PPs in M-AIR, M-cells were also activated by paired, conditioning-test stimuli with an interval of 8 s. This protocol was employed to reduce synaptic efficacy at M-cell output synapses (Curti et al. 2006; Waldeck et al. 2000) and thus, to decrease the M-cell-dependent excitatory drive to prepacemaker neurons in responses evoked by the test stimulus of each pair. Under these conditions, local application of relatively small volumes of blocker solutions will prevent the recruitment of a comparatively larger population of medullary prepacemaker cells during M-AIR. Paired M-cell stimuli were applied at regular intervals (3 min) before and after specific blockade of PPs.

Lesion and pharmacological blockade experiments. In order to exclude diencephalic PPs from the putative neural circuit responsible for organizing the M-AIR (see Fig. 7B), we carried out a complete brainstem transection at the caudal limit of the tectum using a dissecting scalpel blade. In addition, for transient blockade of restricted portions of PPs, glutamate antagonists (±)-2-

amino-5-phosphonopentanoic acid (AP5, 500 μM) combined with 6-cyano-7-nitroquinoxaline-2,3-dione HBC-complex (CNQX, 500 μM), dissolved in NaCl (154 mM), were pressure ejected (30 psi, 50-300 ms), usually unilaterally, into the diencephalon, the octavolateral area and within the caudal medulla. In these experiments, approximate coordinates in the rostrocaudal, lateral and vertical directions of sites of maximal EOD responses to Glu application were first determined; thereafter, microdroplets of antagonist solutions of about 100 μm diameter (measured in air) were applied at these locations. In some experiments, the possibility of unwanted diffusion of blockers onto the PPs-pacemaker cells synapse was assessed by monitoring EOD accelerations elicited by local Glu pressure application (10-20 psi, 50-100 ms) in the vicinity of PM-cells. Glutamate, AP5 and CNQX were obtained from SIGMA-Aldrich (St. Louis, MO, USA).

The peak amplitude of M-AIR was measured before and after surgical pharmacological blockade of PPs. In addition, because the full duration of M-AIR may be indirectly affected by changes in M-AIR amplitude, we calculated the decay time constant (τ_{DEC}) of the response. For this purpose, M-AIR decay phase was fitted with a single exponential function using Clampfit routines of PClamp 8.0 software (Axon Instruments, Foster City, CA, USA). Changes in both peak amplitude and τ_{DEC} were expressed as percentage of controls.

Statistical analysis. For assessing the statistical significance of changes produced by drug or lesion-induced conditions, the two-tailed paired Student *t* test was used. Unless otherwise indicated, summary data are expressed as mean ± standard deviation (SD).

RESULTS

Identification of PPs.

In the present study, the term prepacemaker is applied to specific neuronal populations that project directly upon the PMn *and* modulate the activity of PMn and hence of EODs. Accordingly, our first series of experiments were aimed at identifying putative PPs *via* both morphological and functional criteria.

-Retrograde tracing experiments

Previous work indicates that PM-cells are the exclusive cellular target for glutamatergic afferents involved in M-AIR (Curti et al. 1999, 2006). Accordingly, biocytin was iontophoresed at the PMn where PM-cells are located in 8 animals. The micropipette filled with biocytin solution was used for both extracellular recording and iontophoresis (Fig. 1A). The exact location of the biocytin-filled micropipette relative to the different cell types that comprise the PMn was assessed by the waveform of the field potential produced by the spontaneous pacemaker activity. This field potential is phase-locked with and precedes each EOD (Curti et al. 2006). In *Gymnotus omarorum*, pacemaker and relay cells are spatially segregated within the PMn; whereas PM-cells concentrate within the dorsal aspects of the nucleus, relay cells occupy its ventral portion (Fig. 1B, left). In the vicinity of PM-cells, near the center of the nucleus in the rostro-caudal axis, field potentials elicited by pacemaker activity are characterized by two successive negative-going waves with specific amplitudes and time courses (Fig. 1B, right; see Curti et al. 2006). Examination of the injection sites invariably showed that the marker was present almost exclusively within the location of PM-cells (Fig. $1C_1$). Although biocytin was iontophoresed near the

247 rostro-caudal center of the PMn, extracellular deposits of the marker as well as
248 several labeled PM-cells somas were consistently observed throughout the
249 rostro-caudal extent of the nucleus (Fig. 1C_2).

250 The number of labeled neurons per animal was relatively small (mean =
251 33, range = 7-158) and were systematically observed at the diencephalon, the
252 octavolateral area and the caudal medulla. Representative examples are
253 illustrated in Fig. 2. At the diencephalic level (Fig. 2A), labeled neurons were
254 located in a region that lies ventrolaterally to the nucleus centralis posterior (CP)
255 of the thalamus and laterally to the periventricular nucleus of the posterior
256 tuberculum (nTPP). The shape and diameter of the somas as well as the
257 appearance of their dendritic arbors varied considerably. Although most labeled
258 cells (up to 80%) exhibited small ovoid somas (mean diameter of 11.6 μm, SD
259 ±3.6 μm), a few multipolar cells with larger somas (mean diameter of 19.3 μm,
260 SD ±1.0 μm) were also consistently observed. Ovoid and multipolar cells
261 appeared intermingled without an apparent topographical organization.

262 In the octavolateral area, a region located laterally and dorsally to the M-
263 cell somas (Fig. 2B), labeled neurons were observed in the medial aspects of
264 the medial octavolateral nucleus (MON). In this region, most of the labeled cells
265 exhibited relatively large somas (mean diameter 17.8 μm, SD ±3.3 μm) and
266 dendritic arbors that extended mainly in a ventral and lateral direction, towards
267 the magnocellular octavolateral nucleus.

268 Labeled neurons in the caudal medulla were distributed along a bilateral
269 rostro-caudal column located in an intermediate zone lateral to the medial
270 longitudinal fasciculus at the dorsal limits of the reticular formation (Fig. 2C).

Their somas were moderately elongated (mean diameter of 19.6 μm, SD ±4.6 μm) and exhibited thin dendrites that projected in a dorsal and lateral direction.

Results from retrograde tracing experiments are summarized in Fig. 3. In the rostro-caudal axis, labeled cells were distributed unevenly along a bilateral column that extended from the diencephalon, in the proximity of the CP of the thalamus, to an area located near the rostral pole of the PMn (Fig. 3A). In the frontal plane, the location of labeled neurons observed in all animals (n = 6) is illustrated by the shaded areas in three representative transversal sections (Fig. 3B-D). Marked neurons in close association with the CP of the thalamus (Fig. 3B), most likely encompass the diencephalic prepacemaker nucleus that has been described in most gymnotiform fish (Heiligenberg et al. 1981; Kawasaki et al. 1988; Keller et al. 1991; Kennedy and Heiligenberg 1994). In contrast, labeled neurons located at the octavolateral area, in the vicinity of M-cell somas (Fig. 3C), and at the caudal medulla (Fig. 3D) were not included in previous descriptions of prepacemaker neurons in gymnotiform fish (ibid).

In 3 out of 6 animals, few labeled neurons (in total 18) were also present in a brainstem region approximately 1000 μm rostral to M-cells, lateral to the locus coeruleus and the subcoeruleus nucleus, and ventral to the paralemniscal nucleus near the dorsal boundaries of the mesencephalic reticular formation (not shown).

-Activation of putative PPs by glutamate.

The anatomical evidence obtained by retrograde labeling following biocytin injection into the PMn strongly suggests that several neuronal groups control the activity of this nucleus in *Gymnotus omarorum*. However, in order to be postulated as PPs, the activation of these neuronal groups must induce

evident short-latency modulations of PMn discharge that are usually detected as changes in the frequency or waveform of EODs (Juranek and Metzner 1998; Kawasaki and Heiligenberg 1990). Therefore, in order to verify if the populations of neurons that were retrogradely labeled in the diencephalon, octavolateral area, and caudal medulla play a PP role, we carried out local microinjections of glutamate in these regions in conjunction with EOD recording.

Representative examples of maximal responses evoked by Glu ejection within the three regions explored are illustrated in Fig. 4. Along a vertical track located ~~at~~ 650 µm laterally to the midline at the diencephalon, the maximal response was observed at a depth of 2600 µm and consisted of a short-latency increase in EOD rate (up to 6 Hz) that lasted at least 2.5 s (Fig. 4A1). From this site, the amplitude of the response decreased to a 37% of the maximum response at a level located 600 µm dorsally and almost disappeared at a location situated 200 µm ventrally (Fig. 4A2). Systematic exploration of Glu sensitivity at this region in 7 animals showed that maximal responses were observed at a mean depth of 2800 µm (SD ±160 µm) from brain surface. In all cases Glu provoked increases in EOD rate without changes in EOD waveform. In Fig. 4A3, sites of maximal responses observed in these experiments (black dots) are depicted in a diencephalic coronal section according to their lateral and vertical coordinates. Maximal Glu-responsive sites overlap with the region of labeled neurons observed at the diencephalon near the thalamic CP (see Fig. 3B). In 3 animals Glu sensitivity was also explored at more dorsal locations along vertical tracks (see inset in Fig. 4A3 for a representative example). Another region at which Glu ejection evokes significant increases in EOD rate (up to 80% from maximum although with a slower time rise) was detected at a

depth range of 1700 - 2100 μm from the surface of the brain (grey spots in Fig. 4A3). Responses produced by Glu ejection within this region most likely resulted from activation of neural elements encompassing the medial region of the torus semicircularis ventralis.

Systematic exploration of Glu sensitivity at the octavolateral area was facilitated because the M-cells, which can be easily recognized electrophysiologically (Borde et al. 1991; Faber and Korn 1978; Furshpan and Furukawa 1962), served as a topographical reference in this region of the brainstem. The tip of a Glu pipette, also used to perform extracellular recordings, can be placed deeply in the brainstem at known distances from the M-cell axon cap (Furshpan and Furukawa 1962). Along the vertical track that evoked the maximal response, Glu ejection at a depth of 2900 μm (~ 800 μm from midline and 350 μm lateral to M-cell axon cap) produced a short-latency increase in EOD rate of about 8.6 Hz that lasted for 4.9 s (Fig. 4B1). Along the same track, responses were almost absent 300 μm dorsally, decreased gradually (although non-monotonically) towards more ventral ejection sites, and vanished at 700 μm from the site of maximal response (Fig. 4B2). In 16 animals, maximal responses were observed at a mean depth of 2750 μm (SD ±420 μm). Sites of maximal responses observed in these experiments are depicted in a typical coronal section at the level of the M-cells (Fig. 4B3, black dots) according to their lateral and vertical coordinates respect to the M-cell. These sites encompass the octavolateral area i.e., the same region where biocytin retrogradely labeled neurons were present (see Fig. 3C for comparison). In 6 animals, exploration of Glu sensitivity including more dorsal regions also showed responses to Glu ejection (up to 75% of maximum,

346 although with a slower time course), in a depth range of 1500 to 2200 μm (grey
347 dots, Fig. 4B3); a representative example is illustrated in the inset in Fig. 4B3.
348 Responses that followed glutamate application at these more dorsal sites most
349 likely resulted from activation of medial portions of the electrosensory lateral line
350 lobe (ELL).

351 At the caudal medulla, exploration of Glu sensitivity was carried out at
352 three different rostro-caudal levels separated by 500 μm with similar overall
353 results. The tip of the Glu pipette was positioned rostrally to the PMn, which
354 served as reference. Figure 4C illustrates results obtained from a vertical track
355 conducted 500 μm from midline and approximately 1000 μm rostral to the
356 center of the PMn. At a depth of 2800 μm (Fig. 4C1), Glu ejection provoked a
357 short-latency increase in EOD rate of 7.9 Hz that lasted for 3.7 s. Along this
358 vertical track, amplitude of responses decreased non-monotonically in both
359 dorsal and ventral directions and were virtually absent at a distance of 400 μm
360 from the most effective depth (Fig. 4C2). Overall, sites of maximally-induced
361 EOD responses following Glu application within the caudal medulla (6 animals,
362 up to 36 vertical tracks) were located at a mean depth of 2810 μm (SD ±90 μm).
363 Ejection sites that elicited maximal responses are illustrated in a representative
364 coronal section (black dots, Fig. 4C3). The area of Glu sensitivity in the caudal
365 medulla approximately corresponds to the region of labeled neurons (see Fig.
366 3D for comparison). Vertical tracks that explored more rostral levels within the
367 caudal medulla (n=4) detected an additional area of Glu sensitivity at a depth
368 range of 1700-2100 μm (grey dots, Fig. 4C3) which most likely result from
369 activation of the nucleus medialis. An illustrative depth profile including dorsal
370 and ventral Glu-sensitive areas is depicted in the inset in Fig. 4C3.

Structures activated by injections of Glu at relatively dorsal locations in the diencephalon, the octavolateral area and the caudal medulla, are likely involved in the processing of sensory information from different sources (i.e.: ventral torus, ELL, nucleus medialis). Thus, their activation by Glu may evoke EOD rate modulations similar to those observed during sensory-evoked novelty responses.

The role of PPs in M-AIR.

The M-cell-initiated modulation of the active electrosensory neural system, consists of an abrupt and short latency acceleration of EODs (up to 40% increase in rate) which is long lasting (at least 1 s; Curti et al. 2006; Falconi et al. 1997). Its short delay (about 4 ms for synaptic actions at PM-cells) indicates that the pathway between Mauthner and PM-cells includes only a few interposed neuronal structures. One way to investigate *in vivo* the role of PPs in this modulation includes the analysis of M-AIR changes produced by a complete exclusion of PPs from the underlying neural circuit. However, the fact that in *Gymnotus omarorum* PPs are likely represented by a widely distributed bilateral group of neurons extending from the diencephalon to the caudal medulla, precludes any attempt to carry out this kind of experiments. Consequently, the role of selected sectors of PPs in M-AIR was assessed by means of two different technical approaches: i) the exclusion of more rostral PPs by brainstem transection at the level of the caudal limit of the tectum and ii) the transient blockade of restricted portions of PPs (diencephalic region, octavolateral area and caudal medulla) by local application of ionotropic glutamate receptor antagonists. Before surgical or pharmacological blockade of PPs, M-AIRs were as previously described exhibiting mean peak amplitude of

396 9.7 Hz (SD ± 4.4 Hz, n=43), mean total duration of 2.9 s (SD ± 1.3 s, n=43) and
397 mean τ_{DEC} of 0.67 s (SD ± 0.40 s, n=43).

398 ***- Diencephalic PPs.***

399 According to the putative neural circuit that controls M-AIR (see Fig. 7A),
400 the contribution of most rostral PPs to M-AIR, i.e., diencephalic PPs, is
401 expected to be eliminated by a complete transversal section of the brainstem at
402 the caudal limit of the tectum (see for a scheme Fig. 5A). Accordingly, M-AIR
403 was examined before and after brainstem transection in 9 animals.

404 EOD frequency usually increased (7-10 Hz) immediately after
405 transection, returned to control values in about 2 min and remained stable for
406 the remaining of the experiment (up to 90 min). Modifications of M-AIR were
407 evaluated after complete recovery of EOD basal frequency. As illustrated in Fig.
408 5B, the peak amplitude of M-AIR was reduced to 91.4% of control (from 7.7 Hz
409 to 6.8 Hz) by brainstem transection while the duration of the response
410 decreased from 2.3 s to 0.97 s with a reduction of τ_{DEC} to a 36.6% of control.
411 These changes persisted for the remaining of the experiment (i.e.: 90 min).
412 Similar results, although reversible, were obtained by bilateral local application
413 of CNQX-AP5 solutions at the level of diencephalic PPs (11 injections, 7
414 animals). As shown in Fig. 5C, after bilateral injections of glutamate antagonists
415 (100 ms, 30 psi) into the region of diencephalic PPs, M-AIR shortened, with a
416 decrease of τ_{DEC} to a 33.4% of control whereas peak amplitude showed a
417 reduction to a 91.6% of control. These effects slowly reversed and M-AIR
418 recovered control parameters in about 75 minutes (range 50-90) after injections.
419 Results from brainstem transection and from CNQX-AP5 bilateral application at
420 diencephalic PPs are summarized in Fig. 5D (n=20). Blockade of diencephalic

PPs produced a marked reduction of the duration of M-AIR with a decrease of τ_{DEC} to a mean value of 52.1% (SD ±28.1%) of control, with minor effects on its peak amplitude (mean peak amplitude after blockade 99.1%, SD ±25.1% of control). Whereas changes in M-AIR τ_{DEC} reached statistical significance (p=0.0013), those observed in peak amplitude did not (p=0.4).

- Medullary PPs.

Because of their scattered distribution along an extended area between the PMn and the vicinity of M-cells, the role of medullary PPs on M-AIR was investigated only by local application of CNQX-AP5 solution at the octavolateral area and at two discrete regions located at known distances (500 µm and 1000 µm) from the PMn in the rostral direction and at 500-600 µm from midline.

In a first series of experiments (7 animals), M-AIR was evoked at regular intervals (typically 3 minutes) and its peak amplitude and duration were monitored before and after a single injection of Glu antagonists at a given location. From a total of 29 injections, minimal reversible changes in M-AIR were observed only in 4 injections (13.8%). In these cases M-AIR peak amplitude (but not duration or τ_{DEC}) was slightly reduced to 92.2% of controls (SD ±9.3%, p=0.003). The lack of effect following most of Glu antagonist injections (86.2%) may have been due to the possibility that the number of PPs neurons effectively blocked was not sufficiently large to produce evident effects on M-AIR. As described for most M-cell output pathways (Faber et al. 1989), PPs neurons may be activated by synapses with a high efficacy and probably are part of a highly redundant pathway. In line with this assumption, and considering that activation of M-cell associated circuits is reduced by repetitive M-cell activation (Curti et al. 2006; Faber et al. 1989; Waldeck et al. 2000), the

effect of injections of Glu blockers at medullary PPs on M-AIR was reexamined (21 animals) using repetitive M-cell stimulation in order to reduce synaptic efficacy at M-cell output pathways. Instead of using prolonged repetitive M-cell stimulation which produces a marked suppression of M-AIR (Curti et al, 2006), we designed a stimulation protocol directed to moderately reduce synaptic efficacy at M-cell output pathways without significantly affecting either M-AIR peak amplitude or duration. This was achieved by using paired, conditioning-test stimulation of M-cells with an interval of 8 s. This was confirmed in selected experiments (n=4) by simultaneously recording the M-AIR and the so-called "extrinsic hyperpolarizing potential" (EHP), an electrical event that reflects synchronous activation (burst of action potentials) of a population of recurrent inhibitory interneurons (Borde et al. 1991; Charpier et al. 1994; Faber and Korn 1978; Furukawa and Furshpan 1963). Paired M-cell activation reduced synaptic efficacy at the recurrent inhibitory circuit (Fig. 6A; EHP, lower panel), as indicated by a slight increase in the latency of EHP (108.3%, SD ±4.1%, p=0.145) and a reduction of its amplitude (third peak decreased to a 77.9% of control, SD ±5.7%, p=0.038), while M-AIRs produced by both conditioning and test stimuli were similar (M-AIR, upper panel, p=0.279 and p=0.357, for peak amplitude and $\tau_{DEC,}$ respectively).

Effects of blockade of medullary PPs were then assessed by monitoring peak amplitude and τ_{DEC} of M-AIRs provoked by the test stimulus of each pair prior to and after a single injection of Glu antagonists. Under this condition, injections of blockers were effective in 43 out of 48 injections (89.6%). An example of Glu antagonists-induced changes in M-AIR is shown in Fig. 6B wherein the injection of blockers at a site 1000 μm rostral to the PMn produced

a reduction of peak amplitude of M-AIR to a 77% of control (6 minutes after injection), an effect that vanished ~~at~~ 52 minutes after injection. A summary of results (21 animals, 43 injections) is illustrated in Fig. 6C. Compared to control conditions, there was a reduction in the M-AIR peak amplitude to a mean value of 80.2% (SD ±15.1%, $p<0.0001$); this reduction was observed after a mean interval of 11 min (range 5-16) with a mean recovery time of 98.5 min (range 40-170). In contrast, although reduction of M-AIR peak amplitude was often accompanied by a decrease in total duration, τ_{DEC} was not affected by medullary PPs blockade (106.4%, SD ±47.8%, $p=0.58$).

Injections of Glu antagonist within the PPs at the caudal medulla that produced a transient reduction of M-AIR peak amplitude did not affect the response to Glu (10 mM) on EOD rate when applied near PM-cells at the PMn (n=3, supplemental Fig.1).

DISCUSSION

PPs in Gymnotus omarorum

The present study provides the first description of PPs in *Gymnotus omarorum*. After application of the tracer at the PMn, retrograde-labeled cells distributed unevenly within a bilateral rostro-caudal column that extended from the diencephalon to the caudal medulla (Fig. 3). Marked neurons tended to aggregate near the CP in the thalamus and in the octavolateral area. Although more dispersed, a third group of labeled cells appeared in the caudal medulla between the M-cells and the rostral pole of the PMn. In addition, we found that Glu applied in these three areas (diencephalon, octavolateral and caudal medulla) produced short latency and transient increases in EOD rate (Fig. 4).

These results reveal a distribution of PPs in *Gymnotus omarorum* that contrasts with data previously reported vis a vis the distribution of PPs in other gymnotiform fish (Heiligenberg et al. 1981; Kawasaki and Heiligenberg 1989; Kawasaki et al. 1988; Keller et al. 1990, 1991; Kennedy and Heiligenberg 1994). Prepacemaker neurons have been grouped in two bilateral aggregates located in the diencephalon and mesencephalon, which have been designated as the diencephalic (PPn) and the sublemniscal (sPPn) prepacemaker nuclei, respectively.

It seems unlikely that the neuronal labeling at unforeseen medullary PPs may have resulted from nonspecific labeling caused by extensive diffusion of tracer from the site of injection. As can be concluded from the close examination of the injection site within the PMn in our tracing experiments, the tracer was exclusively present within PM-cells (see Fig. 1C and Results section). Moreover, modulations of EOD rate produced by activation of neuronal

groups located in the octavolateral area and the caudal medulla (Fig. 4B and C) strongly suggest that these neurons are also functionally prepacemaker cells. The small number of labeled cells per animal as well as the fact that they were distant from the site of injection of the marker further confirms the notion that the biocytin-labeled neurons innervate the PMn. However, nonnspecific labeling, if any, cannot be completely ruled out due to uptake of biocytin by some damaged fibers of the medial longitudinal fasciculus during the descent of the pipette containing the tracer solution to the PMn (see Fig. 1B). It has been proposed that physical damage is necessary for biocytin uptake by fibers of passage during tracing experiments (Vercelli et al. 2000).

PPs: the linkage between the electrosensory system and M-cell related networks.

PPs have been first described as the neural interface between sensory systems and the electrogenic component of the active electroreceptive neural system responsible for the organization of sensory evoked EOD modulations (Giassi et al. 2007; Heiligenberg et al. 1981; Kawasaki et al. 1988; Keller et al. 1990; Metzner 1999). However, tract-tracing techniques (see for example, Wong 1997 and for a review Zupanc 2002) also revealed that a wide variety of non-sensory central structures project to PPs. Consequently, PPs might also integrate inputs arising from non-sensory related areas to promote specific EOD modulations. In the present study we demonstrate that, in addition to their role in the organization of sensory evoked EOD modulations, PPs in gymnotiform fish may also participate in the organization of the M-AIR, a modulation of the electrosensory system triggered by a neural signal that takes origin in the M-cell, a central component of the motor neural system responsible for escape.

Based on the latency of M-cell initiated synaptic actions at PM cells (Falconi et al. 1997) and the characteristics of M-cell-evoked field potential near the PMn (Curti et al. 2006) we have previously postulated that a group of as yet unidentified interneurons (Int. in Fig. 7B), similar to cranial relay neurons (CRN) described in goldfish, is interposed between the M-cell axons and PPs. Moreover, location of prepacemaker neurons far away from M-cell axons even for medullary PPs (> 300 μm, present study) together with the fact that M-cell axon in *Gymnotus omarorum* emits few short processes (Trujillo-Cenóz and Bertolotto 1990), probably as those described in goldfish and other teleosts (Funch et al. 1984; Ritter et al. 2001), also suggest that connections between M-cell and PPs neurons are mediated by a group of specialized interneurons.

Results from lesion and local transient blockade experiments (Figs. 5 and 6) indicate that PPs involved in M-AIR are functionally segregated. Whereas diencephalic PPs critically determine the duration of the M-AIR, its peak amplitude relies on the activation of the more caudal PPs. An estimation of their relative contribution to M-AIR is illustrated in Fig. 7A. By point-by-point subtraction of a control M-AIR (upper trace) and a remnant M-AIR after brainstem section (medullary component, middle trace) the contribution of diencephalic PPs (lower trace) can be estimated. The medullary component is relatively brief and mainly responsible for the abrupt increase in rate and peak magnitude of the response whereas the diencephalic component is slow, long lasting and more relevant during the late part of the M-AIR.

A wealth of evidence derived from the study of PPs in several gymnotiform fish strongly suggests that the functional specialization of discrete PPs regions is probable a general organizing principle of prepacemaker

560 networks (Kawasaki and Heiligenberg 1990; Kennedy and Heiligenberg 1994;
561 see also Caputi et al. 2005). Moreover, each subdivision appears to be
562 activated independently during a definite behavioral display. However, our data
563 suggest that the motor command arising from the M-cell may result in
564 simultaneous activation of PPs with apparently disparate functional
565 specialization (Figs. 7B and C). Massive recruitment of different PPs during M-
566 AIR overriding a more precise and probably behavior-related pattern of PPs
567 activation indicate a well-demonstrated general functional characteristic of M-
568 cell dependent circuits (Eaton et al. 2001; Korn and Faber 2005). Convincing
569 physiological evidence indicates that there is a priority of the escape reaction
570 over other motor behaviors (Svoboda and Fetcho 1996) due to a high–safety
571 factor at all connections downstream from the M-cell (Fetcho 1991).

572 ***M-AIR: the modulation of an active sensory system by a motor-derived***
573 ***signal.***

574 A wealth of evidence obtained from both vertebrate and invertebrate
575 experimental models indicates that most neural designs underlying high-level
576 motor-sensory interactions, although with a wide variety of functions, involve the
577 modulation of sensory processing by motor-derived neural signals (Crapse and
578 Sommer 2008; Poulet and Hedwig 2006). However, as reported in the last few
579 years (Friedman et al. 2006; Wilson and Moss 2004), high-level motor-sensory
580 interactions may also include neural designs allowing the modulation of the
581 motor component of the active sensing systems by collaterals of central motor
582 commands leading to adaptive changes of sensory sampling during definite
583 behavioral contexts (Nelson and MacIver 2006). In certain bats, for example,
584 during prey capture, later phases of behavioral displays are accompanied by an

585 increase in the emission rate of echolocating signals which may help fine
586 control of its flight behavior before contact (Wilson and Moss 2004). Similar
587 modulations of active sensing systems during certain motor behaviors have also
588 been reported in rats. During exploration, whisking behavior (Friedman et al.,
589 2006; Grant et al., 2009), a widely used model of active touch in rodents, as
590 well as the frequency of sniffing (Verhagen et al., 2007), display specific
591 changes likely involved in the boosting of the amount of useful sensory
592 information with probable perceptual consequences.

593 The present study shed light on the neural basis of an example of this
594 kind of motor-sensory interaction in a gymnotiform fish. Our data indicate that
595 the modulation of the electrogenic component of the active electrosensory
596 system by a central motor command involves a relatively simple neural pathway
597 that includes the activation of specialized brainstem neurons (PPs) by the
598 command neuron for escape (M-cells) *via* a population of as yet unidentified
599 interneurons (Fig. 8A). This neural design is apparently well suited to increase
600 sensory sampling in close temporal relationship with the motor display. But,
601 what could be the functional role of an enhancement of electrosensory sampling
602 precisely timed with motor escape? A possible answer for this question
603 emerges from the analysis of the correlation of the two concurrent functional
604 consequences of M-cell activation: the M-AIR and the motor escape (Fig. 8B).
605 In most teleosts, the initial component of the escape response (known as the C-
606 start) consists of two successive phases (Eaton et al. 2001). The first phase
607 (stage 1) consists of a highly stereotyped C-bend of the fish body triggered by
608 activation of M-cells. This phase is likely an evasive response that is achieved
609 in approximately 30 ms. The second phase (stage 2) consists in a propulsive

610 turn of the body that begins at the end of the C-bend and most likely results
611 from activation of a population of M-cell-like reticulospinal cells. Several
612 parameters of this motor act, including the escape trajectory, result from
613 integration of multimodal sensory information acquired presumably at the end of
614 the first phase. Although a rigorous kinematic study of escape has not yet been
615 performed in gymnotiforms, preliminary behavioral observations in *Gymnotus*
616 *omarorum* using video recordings, suggest that kinematics of escape responses
617 in this species is similar that of goldfish (Borde et al. 2004). As illustrated in Fig.
618 8B, the start of stage 2 likely occurs during the peak of M-AIR allowing the fish
619 to rapidly update electrosensory information about environment just before the
620 execution of the propulsive phase of escape. The population of M-cell-like
621 reticulospinal cells may then process this information for selecting the escape
622 trajectory. Interestingly, experimental evidence obtained in a related genus
623 strongly suggests that escape responses may be influenced by electrosensory
624 clues (Canfield and Rose 1993).

625 In conclusion, our study contributes to an understanding of the neural
626 basis of a high-level motor-sensory interaction strategy in a vertebrate model
627 characterized by the modulation of the motor component of an active sensory
628 system triggered by a motor command. In *Gymnotus omarorum* this modulation
629 likely represents an enhancement of the fish sampling capability of the
630 environment during M-cell-initiated motor behaviors that provides crucial
631 electrosensory information for an adequate selection of the escape trajectory.
632

ACKNOWLEDGMENTS: We thank Claudio Rivero, Atilio Falconi and Sebastián Curti, although during different periods, for their assistance in some pilot lesion and pharmacological experiments. We are grateful to Drs. Washington Buño, Omar Macadar and Jack Yamuy for their valuable suggestions regarding the manuscript and assistance in English editing. We also thank Dr. José Antonio Muñoz Cueto for his expert advice in the interpretation of results from labeling experiments. This work was partially supported by BID-CONICYT Grant Nº 353, PDT Grant Nº S/C/IF/54/090, CSIC-UdelaR Grant and PEDECIBA-URUGUAY.

642 **REFERENCES**

643 **Barrio LC, Caputi A, Crispino L, Buño W.** Electric organ discharge frequency
644 modulation evoked by water vibration in *Gymnotus carapo*. *Comp Biochem*
645 *Physiol* 100A: 555-562, 1991.

646 **Bell CC**. Sensory coding and corollary discharge effects in mormyrid electric
647 fish. *J Exp Biol* 146: 229-253, 1989.

648 **Borde M, Curti S, Comas V, Rivero C.** Central modulation of a sensory
649 system by a motor command. One intention with two results. *Rev Neurol* 38:
650 253-260, 2004.

651 **Borde M, Pereda AE, Morales FR**. Electrophysiological characteristics of the
652 Mauthner cell of the weakly electric fish *Gymnotus carapo*. *Brain Res* 567: 145-
653 148, 1991.

654 **Canfield JG, Rose GJ.** Electrosensory modulation of escape responses. *J*
655 *Comp Physiol A* 173: 463-474, 1993.

656 **Caputi AA.** Contributions of electric fish to the understanding sensory
657 processing by reafferent systems. *J Physiol Paris* 98: 81-97, 2004.

658 **Caputi AA, Carlson B, Macadar O.** Electric organs and their control. In:
659 *Electroreception*, edited by Bullock TH, Hopkins CD, Popper A, Fay R. New
660 York: Springer, 2005.

661 **Charpier S, Behrends JC, Chang YT, Sur C, Korn H.** Synchronous bursting in
662 a subset of interneurons inhibitory to the goldfish Mauthner cell: synaptic
663 mediation and plasticity. *J Neurophysiol* 72: 531-41,1994.

664 **Crapse TB, Sommer MA.** Corollary discharge across the animal kingdom. *Nat*
665 *Rev Neurosci* 9: 587-600, 2008.

Curti S, Comas V, Rivero C, Borde M. Analysis of behavior-related excitatory inputs to a central pacemaker nucleus in a weakly electric fish. *Neuroscience* 140: 491-504, 2006.

Curti S, Falconi A, Morales FR, Borde M. Mauthner cell-initiated electromotor behavior is mediated via NMDA and metabotropic glutamatergic receptors on medullary pacemaker neurons in a gymnotid fish. *J Neurosci* 19: 9133-9140, 1999.

Eaton RC, Lee RK, Foreman MB. The Mauthner cell and other identified neurons of the hindbrain escape network of fish. *Prog Neurobiol* 63: 467-485, 2001.

Faber DS, Fetcho JR, Korn H. Neuronal networks underlying the escape response in goldfish. *Ann N Y Acad Sci USA* 563:11-33, 1989.

Faber DS, Korn H. Electrophysiology of the Mauthner cell: basic properties, synaptic mechanisms, and associated networks. In: *Neurobiology of the Mauthner Cell*, edited by Faber DS, Korn H. New York: Raven, 1978.

Falconi A, Borde M, Hernandez-Cruz A, Morales FR. Mauthner cell-initiated abrupt increase of the electric organ discharge in the electric fish *Gymnotus carapo*. *J Comp Physiol A* 176: 679-689, 1995.

Falconi A, Lorenzo D, Curti S, Morales FR, Borde M. Mauthner cell-evoked synaptic actions on pacemaker medullary neurons of a weakly electric fish. *J Comp Physiol A* 181: 143-151,1997.

Fetcho JR. Spinal network of the Mauthner cell. *Brain Behav Evol* 37:298-316, 1991.

Friedman WA, Jones LM, Cramer NP, Kwegyir-Afful EE, Zeigler HP, Keller A. Anticipatory activity of motor cortex in relation to rhythmic whisking. *J Neurophysiol* 95: 1274-1277, 2006.

Funch PG, Wood MR, Faber DS. Localization of active sites along the myelinated goldfish Mauthner axon: morphological and pharmacological evidence for saltatory conduction. *J Neurosci* 4: 2397-2409, 1984.

Furshpan EJ, Furukawa TJ. Intracellular and extracellular responses of the several regions of the Mauthner cell of the goldfish. *J Neurophysiol* 25: 732-771, 1962.

Furukawa TJ, Furshpan EJ. Two inhibitory mechanisms in the Mauthner neurons of goldfish. *J Neurophysiol* 26: 140-176, 1963.

Giassi AC, Corrêa SA, Hoffmann A. Fiber connections of the diencephalic nucleus tuberis anterior in the weakly electric fish, *Gymnotus cf. carapo*: an in vivo tract-tracing study. *J Comp Neurol* 503: 655-667, 2007.

Grant RA, Mitchinson B, Fox CW, Prescott TJ. Active touch sensing in the rat: anticipatory and regulatory control of whisker movements during surface exploration. *J Neurophysiol* 101(2): 862-874, 2009.

Heiligenberg W, Finger T, Matsubara J, Carr C. Input to the medullary pacemaker nucleus in the weakly electric fish, *Eigenmannia* (Sternopygidae, gymnotiformes). *Brain Res* 211: 418-423, 1981.

Horikawa K, Armstrong WE. A versatile means of intracellular labeling: injection of biocytin and its detection with avidin conjugates. *J Neurosci Methods* 25: 1–11, 1988.

Juranek J, Metzner W. Segregation of behavior-specific synaptic inputs to a vertebrate neuronal oscillator. *J Neurosci* 18: 9010-9019, 1998.

Kawasaki M, Heiligenberg W. Distinct mechanisms of modulation in a neuronal oscillator generate different social signals in the electric fish, *Hypopomus*. *J Comp Physiol A* 165: 731-741, 1989.

Kawasaki M, Heiligenberg W. Different classes of glutamate receptors and GABA mediate distinct modulations of a neuronal oscillator, the medullary pacemaker of a gymnotiform electric fish. *J Neurosci* 10: 3896-3904, 1990.

Kawasaki M, Maler L, Rose GJ, Heiligenberg W. Anatomical and functional organization of the prepacemaker nucleus in gymnotiform electric fish: the accommodation of two behaviors in one nucleus. *J Comp Neurol* 276: 113-131, 1988.

Keller CH, Kawasaki M, Heiligenberg W. The control of pacemaker modulations for social communication in the weakly electric fish *Sternopygus*. *J Comp Physiol A* 169: 441-450, 1991.

Keller CH, Maler L, Heiligenberg W. Structural and functional organization of a diencephalic sensory-motor interface in the gymnotiform fish, *Eigenmannia*. *J Comp Neurol* 293: 347-376, 1990.

Kennedy G, Heiligenberg W. Ultrastructural evidence of GABA-ergic inhibition and glutamatergic excitation in the pacemaker nucleus of the gymnotiform electric fish, *Hypopomus*. *J Comp Physiol A* 174: 267-280, 1994.

Korn H, Faber DS. The Mauthner cell half a century later: a neurobiological model for decision-making? *Neuron* 47: 13-28, 2005.

Lissman HW, Machin KE. The mechanism of object location in *Gymnarchus niloticus* and similar fish. *J Exp Biol* 35: 451-486, 1958.

737 **Lorenzo D, Silva AC, Borde M, Macadar O**. Electrogeneration in South
738 American weakly electric fish. In: *Sensory biology of jawed fishes: new insights*,
739 edited by Kapoor BG, Hara TJ. New Delhi: Oxford & IBH Publishing, 2001.
740 **Maler L, Sas E, Johnston S, Ellis W.** An atlas of the electric fish *Apteronotus*
741 *leptorhynchus*. *J Chem Neuroanat* 4: 1-38, 1991.
742 **McCloskey DJ.** Corollary discharges: motor commands and perception. In:
743 *Handbook of Physiology. Nervous system II*, edited by Brookhart JM,
744 Mountcastle VB, Brooks VB, Geiger SR. Bethesda, Maryland: American
745 Physiological Society, 1981.
746 **Metzner W.** Neural circuitry for communication and jamming avoidance in
747 gymnotiform electric fish. *J Exp Biol* 202: 1365-1375, 1999.
748 **Morales FR, Falconi, A, Hernandez-Cruz A, Borde M.** Abrupt increase in the
749 rate of the electric organ discharge initiated by the Mauthner cell in *Gymnotus*
750 *carapo. J Comp Physiol A* 173: 751, Special Issue, 1993.
751 **Nelson ME and MacIver MA.** Sensory acquisition in active sensing systems. *J*
752 *Comp Physiol A* 192: 573-586, 2006.
753 **Poulet JF, Hedwig B.** The cellular basis of a corollary discharge. *Science* 27:
754 518-522, 2006.
755 **Richer-de-Forges M, Crampton WGR, Albert JS.** A new species of Gymnotus
756 (Gymnotiformes, Gymnotidae) from Uruguay: description of a model species in
757 neurophysiological research. *Copeia* 3: 538–544, 2009.
758 **Ritter DA, Bhatt DH, Fetcho JR.** In vivo imaging of zebrafish reveals
759 differences in the spinal networks for escape and swimming movements. *J*
760 *Neurosci* 21: 8956-8965, 2001.

Santana UJ, Roque-da-Silva AC, Duarte TT, Corrêa SA. Interference with the GABAergic system in the dorsolateral telencephalon and modulation of the electric organ discharge frequency in the weakly electric fish *Gymnotus carapo. J Comp Physiol A* 187: 925-933, 2001.

Sawtell NB, Williams A, Bell CC. From sparks to spikes: information processing in the electrosensory systems of fish. *Curr Opin Neurobiol* 15: 437-443, 2005.

Sommer MA, Wurtz RH. Brain circuits for the internal monitoring of movements. Ann Rev Neurosci 31: 317-338, 2008.

Sperry RW. Neural basis of the spontaneous optokinetic response. *J Comp Physiol Psychol* 43: 482-489, 1950.

Svoboda KR, Fetcho JR. Interactions between the neural networks for escape and swimming in goldfish. *J Neurosci* 16: 843-852, 1996.

Trujillo-Cenóz O, Bertolotto C. Mauthner cells in the medulla of the weakly electric fish *Gymnotus carapo*. *Experientia* 46: 441-443, 1990.

Vercelli A, Repici M, Garbossa D, Grimaldi A. Recent techniques for tracing pathways in the central nervous system of developing and adult mammals. *Brain Res Bull* 51: 11-28, 2000.

Verhagen JV, Wesson DW, Netoff TI, John AWhite, Wachowiak M. Sniffing controls an adaptive filter of sensory input to the olfactory bulb. *Nat. Neurosci*. 10: 631 – 639, 2007

von Holst E, Mittelstaedt H. The reafference principle. Interactions between the central nervous system and the periphery. *Naturwissenchaften* 37: 464-476, 1950. In: *Selected papers of Erich von Holst: The behavioural physiology of animals and man*. London: Methuen. Vol. 1., 1973.

Waldeck RF, Pereda A, Faber DS. Properties and plasticity of paired-pulse depression at a central synapse. *J Neurosci* 20: 5312-5320, 2000.

Webb B. Neural mechanisms for prediction: do insects have forward models? *Trends Neurosci* 27: 278-282, 2004

Wilson WW, Moss CF. Sensory-motor behavior of free-flying FM bats during target capture. In: *Advances in the study of echolocation in bats and dolphins*, edited by Thomas JA, Moss CF, Vater M. Chicago: Chicago University Press, 2004.

Wong CJ. Afferent and efferent connections of the diencephalic prepacemaker nucleus in the weakly electric fish, *Eigenmannia virescens*: interactions between the electromotor system and the neuroendocrine axis. *J Comp Neurol* 383: 18-41, 1997.

Zupanc GK. From oscillators to modulators: behavioral and neural control of modulations of the electric organ discharge in the gymnotiform fish, *Apteronotus leptorhynchus*. *J Physiol Paris* 96: 459-472, 2002.

803 **FIGURE LEGENDS**

804 Figure 1. A. Schematics of the experimental design for retrograde labelling of
805 prepacemaker structures (PPs) showing the pacemaker nucleus (PMn)-
806 composed by pacemaker (PM) and relay (R) cells- innervated by PPs and the
807 micropipette used for both extracellular recording and dye iontophoresis. B.
808 Photomicrograph of the PMn (left) of a representative transversal section
809 approximately through the center of the nucleus depicting the localization of PM
810 and R cells. MLF: medial longitudinal fasciculus. Biocytin was ionophoresed in
811 the vicinity of PM-cells, location indicated by the presence of a typical field
812 potential recording (right). C. Photomicrographs of representative transversal
813 (1) and horizontal (2) sections showing the distribution of tracer deposits at the
814 injection site within the PMn. Note that the dye distributed almost exclusively at
815 the level of PM-cells.

816

817 Figure 2. Camera lucida drawings (left) and photomicrographs (right) of
818 representative transverse sections through the diencephalon (A), the rostral
819 medulla at the level of M-cells (B) and at the caudal medulla (C) illustrating the
820 distribution of retrogradely labeled cells after byocitin deposits near PM-cells at
821 the PMn.
822 A. At the diencephalon labeled cells appeared in the vicinity of the central
823 posterior (CP) thalamic nucleus (left, oblique arrow). The inset at right depicts a
824 photomicrograph at higher magnification obtained from a horizontal section
825 showing a group of labeled cells bodies and several dendritic branches
826 extending rostrolaterally and caudolaterally.

B. At the octavolateral area, marked neurons distributed in a region lateral and dorsal to the M-cells, within or in the close proximity of the medial octavolateral nucleus (left, oblique arrows). The cell body of the M-cell is evident in the photomicrograph at right.

C. In this representative transversal section obtained at about 1000 μm from the PMn in the rostral direction, retrograde labeled cells appeared at the dorsal limit of the reticular formation (left, oblique arrow).

CC: Crista cerebellaris; CP: Central-posterior nucleus; DFl: Nucleus diffusus lateralis of the inferior lobe; ELL: Electrosensory lateral line lobe; M-cell: Mauthner cel; MgVIII: Magnocellular octavolateral nucleus; MLF: Medial longitudinal fasciculus; MON: Medial octavolateral nucleus; PMRF: Paramedian reticular formation; RF: Reticular formation; TA: Nucleus tuberis anterior; TeO: Optic tectum; tVd: Descending trigeminal tract; V: Ventricle

Figure 3. Summary of retrograde labeling in the diencephalon and brainstem after tracer deposits in the vicinity of PM cells at the pacemaker nucleus.

A. Most of labeled cells somas (black dots) observed in our successful retrograde labeling experiments (6 out of 8 animals) were included in a schematic of a representative horizontal section that comprises the diencephalon, the brainstem and the rostral spinal cord. The M-cell bodies and the pacemaker nucleus (PMn), two neural structures that were taken as references in our study are also illustrated. The midline is represented by a dotted vertical line.

B-D Rostral to caudal series of camera lucida drawings of representative transversal sections through the diencephalon, the octavolateral area and the

caudal medulla, three specific levels of the neuraxis selected for analysis (see text). At each level the shaded area (dark grey at ventral right quadrant) represents a hypothetical surface that contains most of labeled neurons observed in 6 animals. Representative section at the caudal medulla corresponds to a region approximately halfway between the PMn and the M-cells. C: Cerebello-medullary cistern; CCb: Corpus cerebelli; CP: Central-posterior nucleus; ELL: Electrosensory lateral line lobe; M-cell: Mauthner cell; MLF: Medial longitudinal fasciculus; MON: Medial octavolateral nucleus; RF: Reticular formation; TeO: Optic tectum; V: Ventricle

Figure 4. EOD modulations produced by activation of putative prepacemaker structures (PPs) by local Glutamate pressure ejection.

A. Exploration of Glu sensitivity at the diencephalon. 1. Plot of EOD frequency versus time of an example of maximal EOD rate response to Glu (10 mM, 20 ms, 15 psi) during a vertical exploratory tract performed at 650 µm from midline. 2. Depth profile of EOD rate responses during the same vertical tract. 3. Sites of maximal Glu sensitivity observed during these experiments are illustrated (black dots) in a quadrant of a schematic drawing of a representative transversal section. Sites of Glu sensitivity identified at more dorsal locations (grey dots) are also represented. Inset, illustrative depth profile of responses to Glu (% of peak amplitude) during an extended exploratory vertical tract (from 1.5 to 3.6 mm). Depth axis, same scale as part 3.

B and C. Same structure as in A but during exploration of Glu sensitivity at the octavolateral area and at the caudal medulla respectively. Depth ranges

explored were 1.4 to 3.3 mm and 1.6 to 3.1 mm for insets in B and C respectively.

For all EOD frequency versus time plots, the moment of Glu ejection is indicated by the arrowhead and dotted line show basal EOD frequency indicated in each trace by the numbers at left.

Figure 5. Recruitment of diencephalic PPs determines the duration of M-AIR.

A. Schematic drawing of a lateral view of the brain of *Gymnotus omarorum*. Lateral line (LLn) and VIII nerves (VIIIn) are also depicted. The approximate location of M-cells and of the PMn was included in the scheme for reference. The vertical dotted line indicate the level at which the brainstem was sectioned during the analysis of the role of diencephalic PPs in M-AIR. Dark grey areas represent the most prominent groups of retrogradely labeled neurons whose activation by Glu evoke short latency EOD accelerations.

B. Plots of EOD frequency versus time of single M-AIRs evoked before (open circles, CONTROL) and 3 min. (filled circles, SECTION) following the complete brainstem section at the level indicated in A.

C. Plots of EOD frequency versus time of single M-AIRs evoked before (open circles, CONTROL), 5 min. (filled circles in black) and 25 min. (filled circles in grey) following bilateral pressure ejection of a solution of glutamate antagonists (AP5 500 µM and CNQX 500 µM in NaCl 154 mM, 30 psi, 100 ms) at diencephalic PPs.

In B and C, the moment of M-cell activation at the spinal cord is indicated by an asterisk and dashed line show basal EOD frequency indicated in each trace by the numbers at left.

D. Summary data (mean ± SD, n=20) of effects of diencephalic PPs blockade on M-AIR amplitude (dark grey bar) and decay time constant (τ_{DEC}, light grey bar) plotted as percentages of their respective control values.

Figure 6. Amplitude of M-AIR results critically from activation of medullary PPs.
A. Paired M-cell activation at 8 s delay does not modify M-AIR but reduces synaptic efficacy at M-cell associated circuits. Upper panel (M-AIR), plots of EOD frequency versus time of M-AIRs elicited by conditioning (filled circle in grey, Cond.) and test (filled circle in black, Test) stimuli of a pair. Lower panel (EHP), superimposed field potential recordings in the vicinity of the left M-cell axon cap in response to the same pair of stimuli (grey line, Cond.,black line, Test) Note that paired M-cell axon activation provoked an increase in latency and a reduction in amplitude of late positive components of evoked field potentials. Antidromic M-cell spikes of about 8 mV were truncated.
B. Plots of EOD frequency versus time of M-AIRs obtained before (CONTROL) and after (intervals indicated over each plot) a bilateral pressure ejection of glu antagonists (AP5 500 μM and CNQX 500 μM in NaCl 154 mM, 25 psi, 300 ms) at medullary PPs.
In A and B the moment of M-cell axon activation is indicated by an asterisk. In B, dashed line show basal EOD frequency indicated by the number at left.
C. Summary data (mean ± SD, n=43 injections) of effects of medullary PPs blockade on the amplitude (dark grey bar) and decay time constant (τ_{DEC}, light grey bar) of M-AIRs evoked by test stimulus of each pair (8s delay) plotted as percentages of their respective control values.

Figure 7. Diencephalic and medullary PPs involved in M-AIR are functionally segregated.

A. Plots of EOD frequency (normalized) versus interval number of a representative M-AIR (M-AIR, upper plot), the remnant M-AIR after a complete brainstem section at the level indicated in Fig. 5A (Medullary component, middle plot) and the result of a point-by-point substraction of these two responses (Diencephalic component, lower plot). See text for explanation. The vertical dotted line indicating the first interval of the control response is included to facilitate comparison between plots.

B. Diagram of the putative neural circuit that mediates M-AIR. The M-cell probably innervates an as yet unidentified group of interneurons (Int.) which in turn innervates diencephalic and medullary PPs. Pacemaker cells, receiving PPs innervation, and R-cells are also depicted. Diencephalic and medullary PPs exhibited different dashing pattern (key included in C) to illustrate their dissimilar functional role in the organization of M-AIR.

C. Schematic drawing of a lateral view of the brain of *Gymnotus omarorum* showing, more realistically, the distribution and functional specialization of PPs involved in M-AIR. As in Fig. 5A, several anatomical details were included in the scheme for reference. Key of their role in the organization of M-AIR is illustrated in the bottom left.

Figure 8. Proposed neural basis and possible functional implications of the modulation of the electrosensory sensory system by an M-cell-derived signal.

A. Diagram of the neural pathway connecting the M-cell and the active electrosensory neural system. For the sake of simplicity, this system is

represented by blocks connected by arrows illustrating the PPs and the PMn as parts of its electrogenic component and central and peripheral structures of its electroreceptive component. A reafferent EOD pathway linking both components at the periphery is also illustrated. The M-cell-derived signal modulates the electrogenic component of the active electrosensory system via a group of interneurons (Int.) innervating the PPs.

B. Schematics of the temporal correlation of M-AIR and the two phases of escape response in teleosts. Plot of EOD frequency versus time of a representative M-AIR in which the approximate timing of the initial components of escape response (according to Eaton et al. 2001) is represented by the dark and light grey rectangles delimited by vertical dotted lines. The dark grey region indicate the stage I (S1) of the response which begins about 12 ms after M-cell activation, lasts for 25 ms and is considered an evasive, relatively stereotyped response that is highly dependent on M-cell activation. The stage 2 (S2) that immediately follows the first stage, is illustrated by the light grey region. This stage lasts for about 45 ms is propulsive, variable and most likely result from activation of a group of M-cell-like reticulospinal neurons. Note that the start of S2 approximately coincides with the peak of M-AIR.

Supplemental figure 1. Demonstration of specificity of PPs blockade by injections of Glutamate antagonists at the caudal medulla.

A. Plots of EOD frequency versus time of test M-AIRs and of EOD accelerations provoked by Glu injections at the PMn (insets), obtained before (CONTROL) and after (intervals indicated over each plot) a unilateral pressure ejection of Glu antagonists (AP5 500 µM and CNQX 500 µM in NaCl 154 mM, 20 psi, 150

ms) at medullary PPs located at 1000 µm from the PMn in the rostral direction. Glutamate (10 mM in NaCl 154 mM) was applied by pressure (10 psi and 20 ms) in the vicinity of PM cells. For comparison, control amplitude of Glu responses is indicated by a short dotted line segment.

Dashed line show basal EOD frequency indicated by the number at left and asterisks indicate the moment of M-cell stimulation.

B. Plot of peak amplitudes versus time of M-AIR (open circles) and Glu responses (filled circles) obtained before and following injection of Glu antagonists at PPs located at the caudal medulla (n=3). Antagonists were injected at time=0.

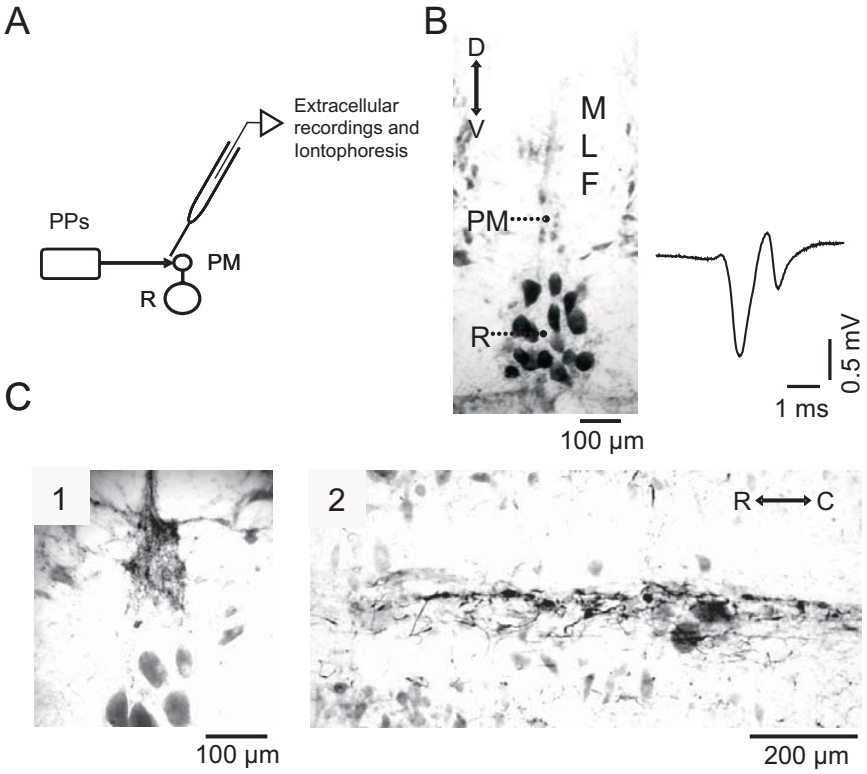
A
Extracellular
recordings and
Iontophoresis
PPs
PM
R
B
D
V
M
L
F
PM
R
100 µm
0.5 mV
1 ms
C
1
100 µm
2
R
C
200 µm

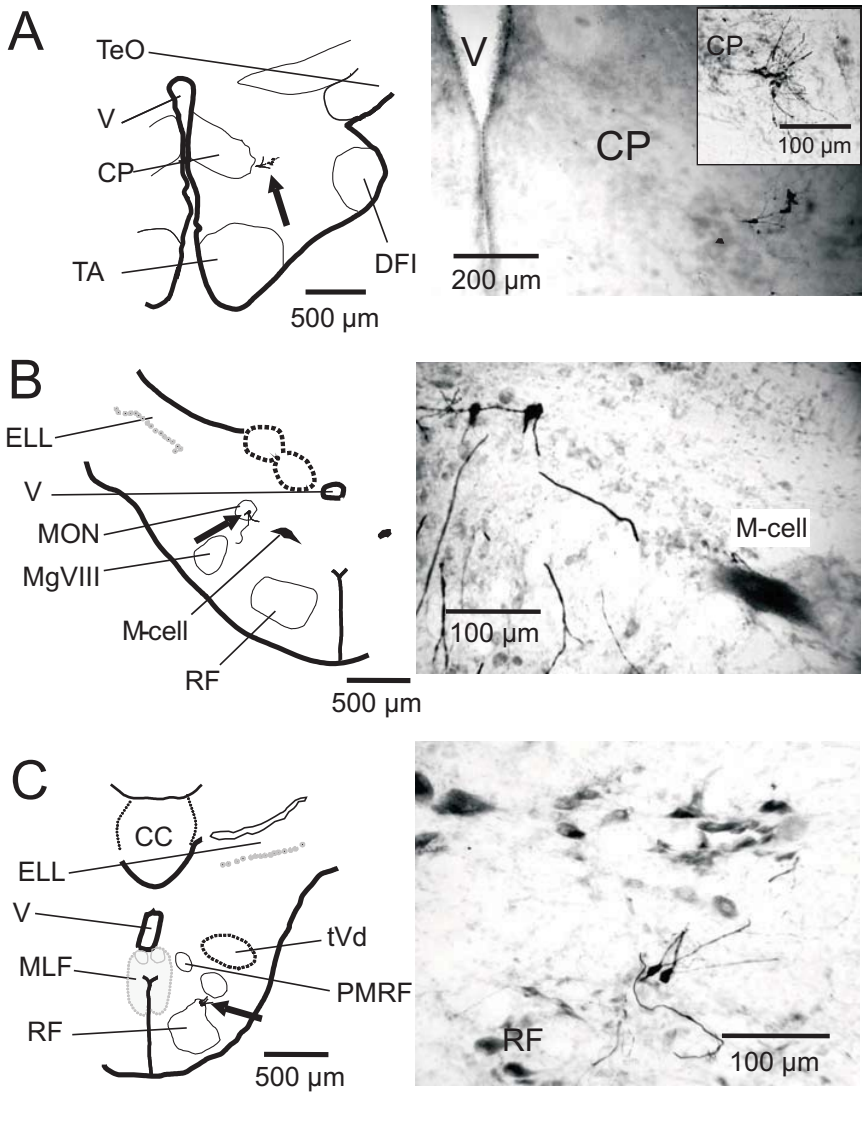
A
TeO
V
CP
TA
DFI
500 µm
V
CP
200 µm
CP
100 µm
B
ELL
V
MON
MgVIII
M-cell
RF
500 µm
M-cell
100 µm
C
CC
ELL
V
MLF
RF
tVd
PMRF
500 µm
RF
100 µm

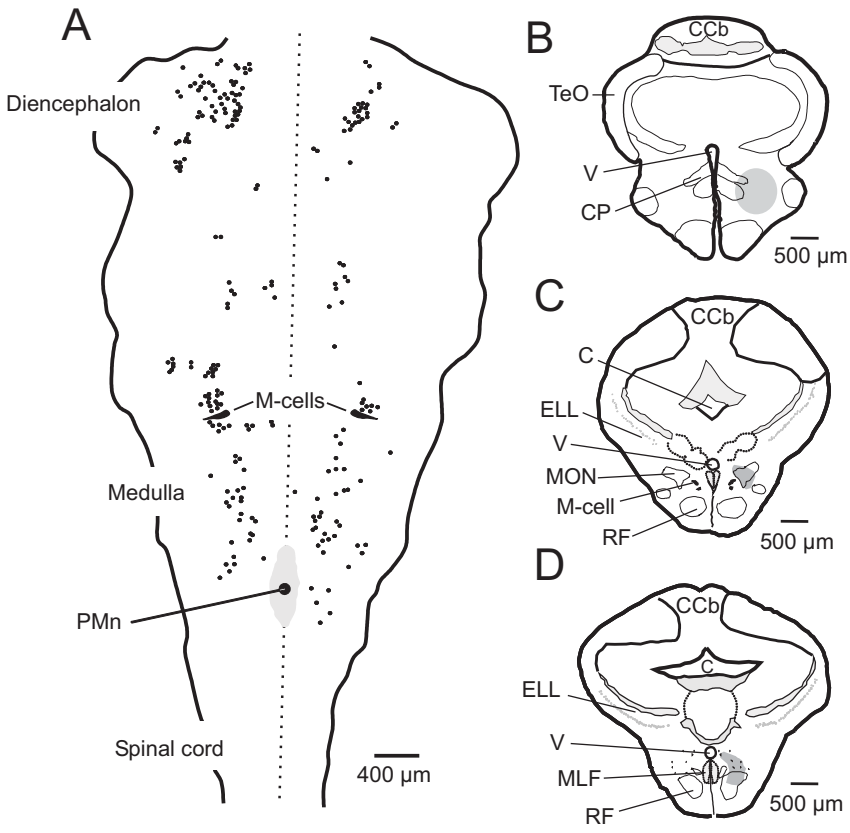
A
Diencephalon
M-cells
Medulla
PMn
Spinal cord
400 µm
B
CCb
TeO
V
CP
500 µm
C
CCb
C
ELL
V
MON
M-cell
RF
500 µm
D
CCb
C
ELL
V
MLF
RF
500 µm

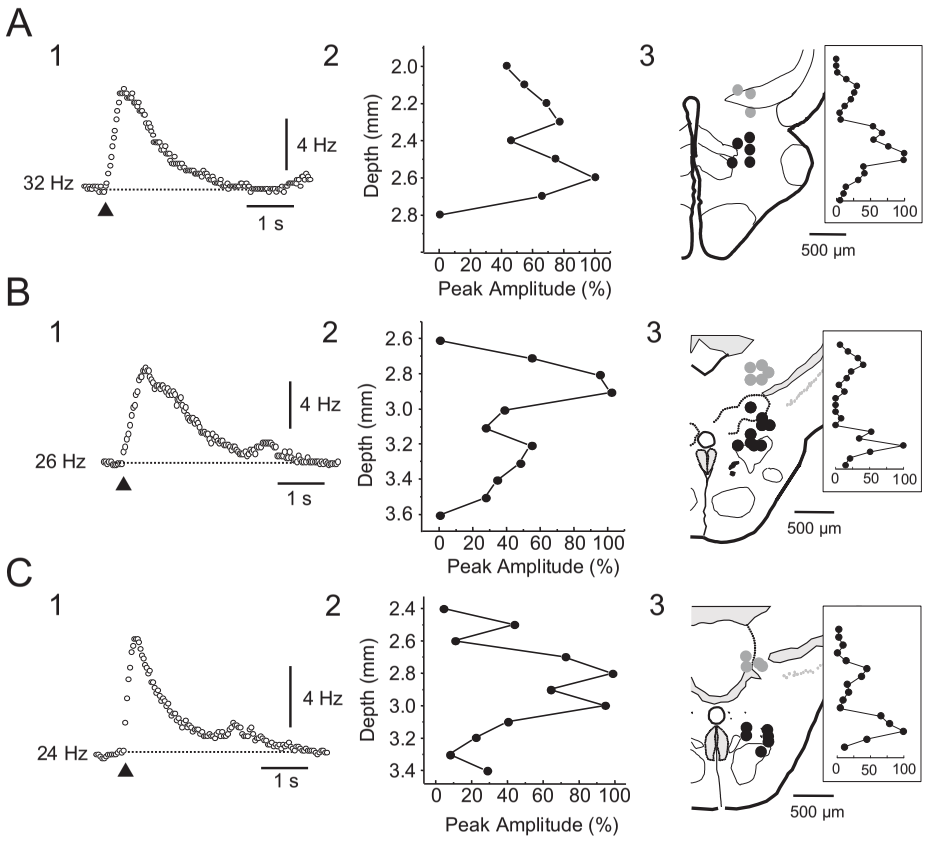
A
1
2
3
4 Hz
32 Hz
1 s
Depth (mm)
2.0
2.2
2.4
2.6
2.8
0 20 40 60 80 100
Peak Amplitude (%)
0 50 100
500 µm
B
1
2
3
4 Hz
26 Hz
1 s
Depth (mm)
2.6
2.8
3.0
3.2
3.4
3.6
0 20 40 60 80 100
Peak Amplitude (%)
0 50 100
500 µm
C
1
2
3
4 Hz
24 Hz
1 s
Depth (mm)
2.4
2.6
2.8
3.0
3.2
3.4
0 20 40 60 80 100
Peak Amplitude (%)
0 50 100
500 µm

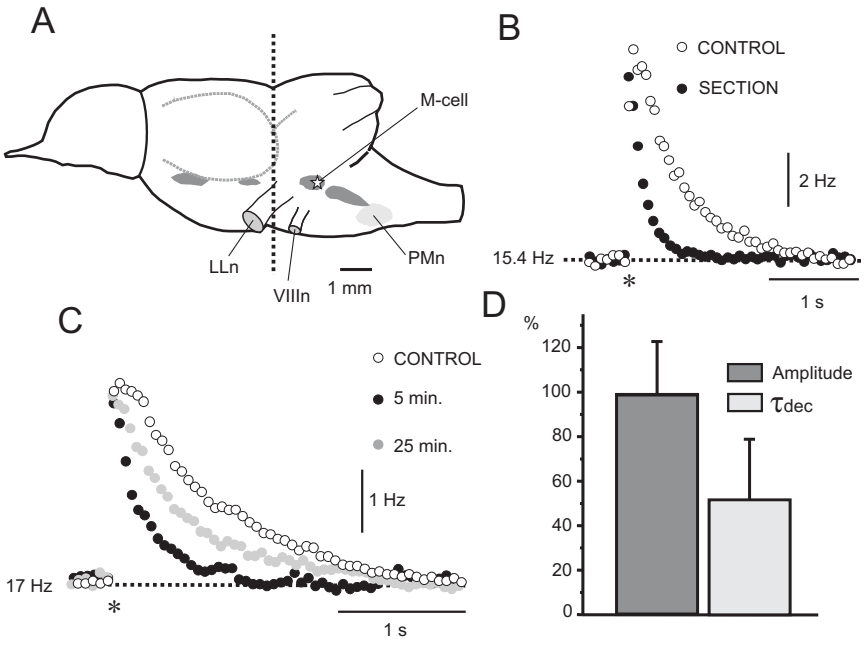
A
M-cell
LLn
VIIIn
1 mm
PMn
B
CONTROL
SECTION
2 Hz
15.4 Hz
1 s
C
CONTROL
5 min.
25 min.
1 Hz
17 Hz
1 s
D
%
120
100
80
60
40
20
0
Amplitude
τdec

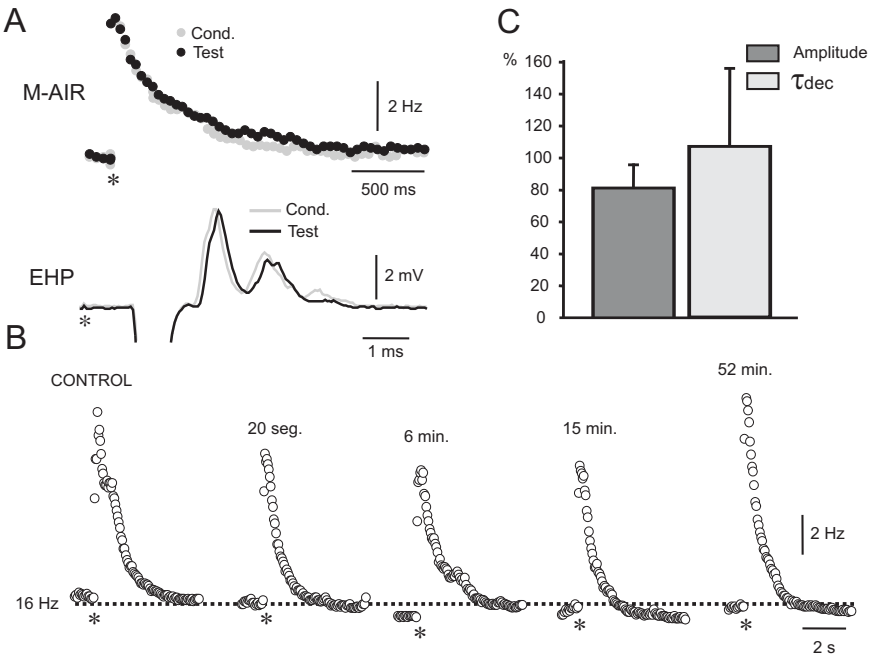
A
Cond.
Test
M-AIR
2 Hz
500 ms
Cond.
Test
EHP
2 mV
1 ms
B
CONTROL
20 seg.
6 min.
15 min.
52 min.
16 Hz
2 Hz
2 s
C
Amplitude
τdec
%
160
140
120
100
80
60
40
20
0

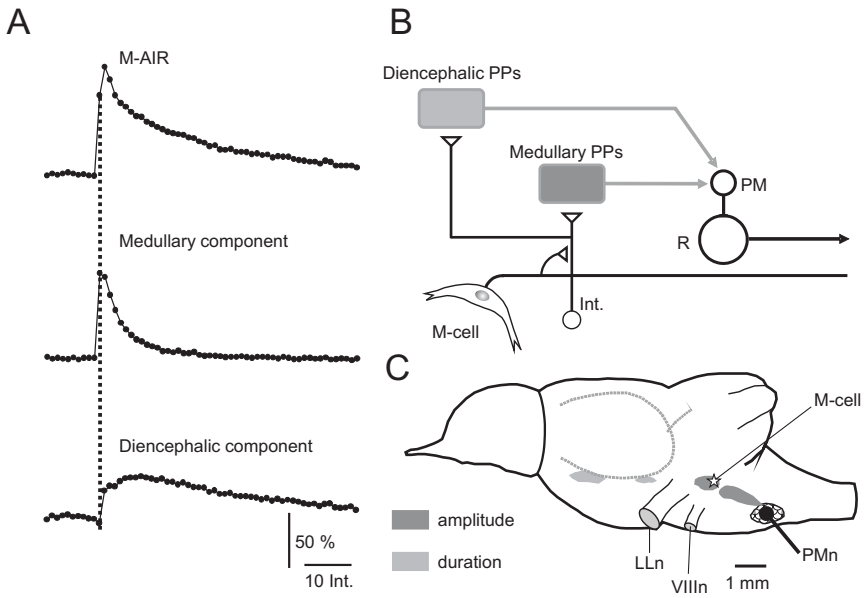
A
M-AIR
Medullary component
Diencephalic component
50 %
10 Int.
B
Diencephalic PPs
Medullary PPs
PM
R
Int.
M-cell
C
M-cell
amplitude
duration
LLn
VIIIn
1 mm
PMn

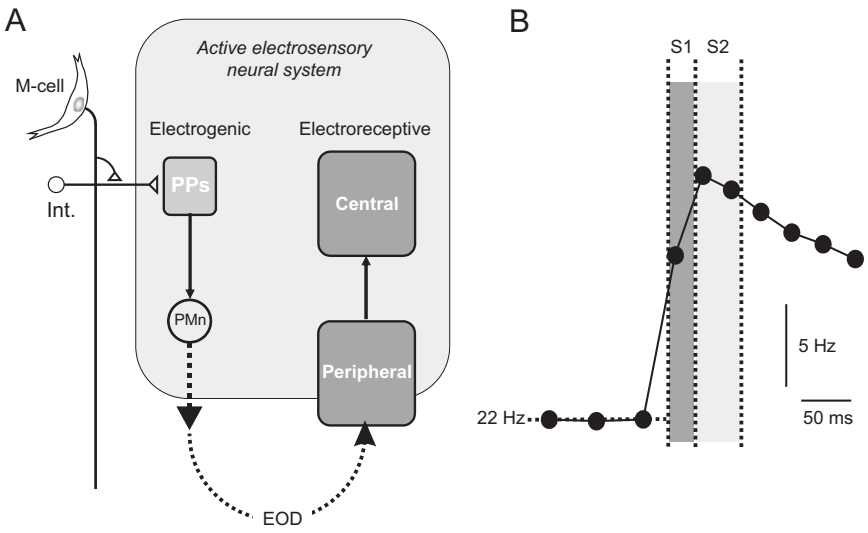
A
Active electrosensory
neural system
M-cell
Electrogenic
Electroreceptive
PPs
Central
Int.
PMn
Peripheral
EOD
B
S1
S2
5 Hz
22 Hz
50 ms

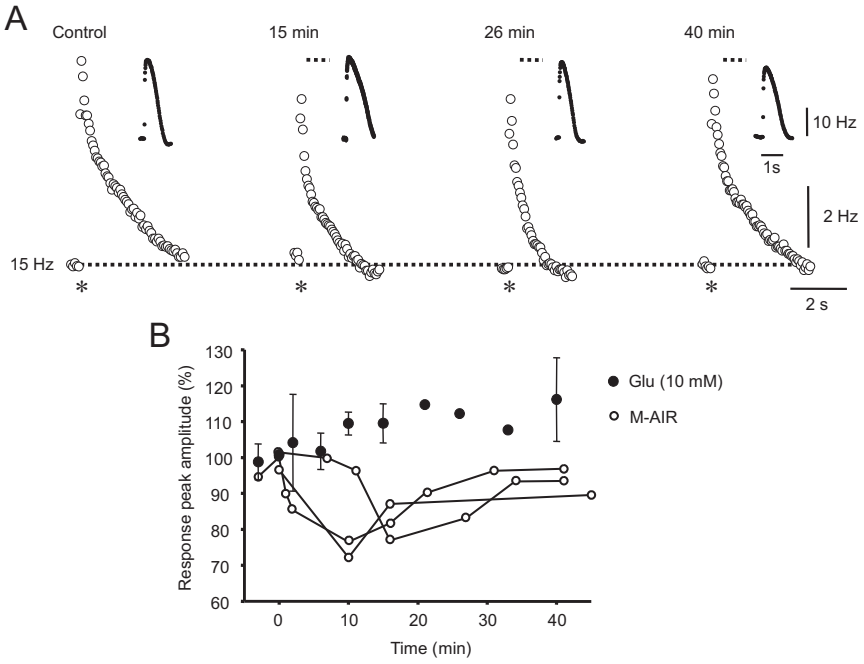
A
Control
15 min
26 min
40 min
10 Hz
1s
2 Hz
15 Hz
2 s
B
Response peak amplitude (%)
130
120
110
100
90
80
70
60
0
10
20
30
40
Time (min)
Glu (10 mM)
M-AIR